Low-Complexity Channel Prediction Using Approximated Recursive DCT

Jorge F. Schmidt, *Member, IEEE*, Juan E. Cousseau, *Senior Member, IEEE*, Risto Wichman, and Stefan Werner, *Senior Member, IEEE*

***Abstract*—We present a novel channel estimator/predictor for OFDM systems over time-varying channels using a recursive formulation of a basis expansion model (BEM) based on an approximated discrete cosine transform (DCT). We derive a recursive implementation of the approximated DCT-BEM for tracking time-varying channels based on a filter bank. The recursive approximated DCT-BEM structure is then used for long range channel prediction by proper scaling and time extrapolation of the filter bank. As the implicit BEM is time invariant we further simplify the implementation by employing a steady-state Kalman filter whose overall complexity is comparable to an LMS algorithm. The derived predictor outperforms, in terms of predictor range, previously proposed long range predictors that are based on autoregressive (AR) modeling of the time-varying channel. For a similar performance, in terms of MSE, the computational complexity of the proposed predictor is significantly lower than conventional sum-of-sinusoids (SOS) channel predictors as no channel delays nor Doppler frequencies need to be estimated.**

***Index Terms*—Basis function approximation, channel prediction, discrete cosine transform, Doppler spectrum, fast-fading channel, Kalman filter, narrowband filters.**

I. Introduction

CHANNEL prediction facilitates efficient sharing of channel resources in wireless communication systems. For example, in long-term evolution (LTE) downlink [1], physical layer scheduler allocates channel resources between users in 2 ms resolution. The resource allocation is based on SNR values reported by the users through a feedback channel. The feedback channel is subject to latency and therefore efficient link adaptation requires prediction of the received SNR around 2 ms ahead. Moreover, channel prediction is indispensable for secondary receivers in cognitive radio systems [2].

Based on [3] and [4], a BEM using discrete prolate spheroidal sequences (DPSS) was proposed in [5] for the estimation of a time varying channel, and the performance of several different basis sets have been studied and compared in [6]. Other BEMs were also reported in [7] and [8] for receiver design in wideband mobile communication systems. Apart from the BEM, time varying channel estimators based on a physical model of the Doppler have been reported in [9], [10] where an AR or an ARMA model is adjusted to fit the Jakes Doppler spectrum [11] and inserted in a Kalman formulation for channel estimation.

BEM estimators are robust to the spectrum shape and thus outperform, in terms of MSE performance, the estimators based on a physical model of the Doppler spectrum in case of model mismatch. However, as the estimation in practice is frame based, the achievable prediction horizon is limited by the basis expansion extension error [12]. On the other hand, following the physical model estimation approach, long range channel predictors have been developed in [13]–[15] exploiting the fact that the signal bandwidth is much larger than the maximum Doppler shift. However, this solution exhibits an error floor due to the mismatch between the Doppler model and that of practical channels which do not always fulfill the Jakes assumption [16]. A review of existing channel prediction approaches is presented in [17] where it is concluded that AR-based predictors perform better than sum-of-sinusoids (SOS) based predictors for short prediction horizons on statistical channel models, while SOS predictors attain larger prediction horizons on synthetic channels. In spite of that, combination of these two approaches has not been reported yet.

In this paper, we propose a recursive-BEM approach for channel estimation and prediction for OFDM. We develop a recursive BEM based on an approximation of the discrete cosine transform (DCT). The benefits of DCT energy compaction property in wireless applications have been reported by many contributions in the past few years [18]–[20] and recently [21]–[26]. Further, Kalman filter proposals for tracking subspace models in different applications context have been reported in [27], [28]. We show that our recursive BEM can be inserted into a Kalman filter formulation, similar to [9], [10], and [29] but with a stationary solution as the recursive modeling of the basis functions is time invariant. This results in a significant complexity saving, because the Kalman gain does not have to be updated, making the proposed approach comparable in terms of complexity with the other BEM proposals [3], [5] and AR-based predictor proposals [14], [15], [30]. At the same time DCT-BEM gives better prediction performance as it achieves larger prediction horizons without exhibiting a model mismatch error floor.

The outline of the paper is as follows. In Section II we define the system model, and introduce the notation. The recursive

Manuscript received June 22, 2010; revised November 05, 2010 and January 04, 2011; accepted February 01, 2011. Date of publication July 14, 2011; date of current version September 28, 2011. This work was supported in part by the Academy of Finland, Smart Radios (SMARAD) Center of Excellence, Agencia Nacional de Promocion Cientifica y Tecnologica PICT 2008-0182, and the University Nacional del Sur, Argentina, under Project 24/K043. This paper was recommended by Associate Editor M. Mondin.

J. F. Schmidt and J. E. Cousseau are with Universidad Nacional del Sur, IIIE-CONICET, Bahía Blanca, Argentina (e-mail: schmidt@uns.edu.ar; jcousseau@uns.edu.ar).

R. Wichman and S. Werner are with Aalto University School of Electrical Engineering, 00076 Aalto, Finland. (e-mail: risto.wichman@tkk.fi; stefan.werner@tkk.fi).

Digital Object Identifier 10.1109/TCSI.2011.2158139

BEM is introduced in Section III. The Kalman filter Doppler estimator is presented in Section IV and the proposed channel predictor is derived in Section V. A computational complexity analysis is presented in Section VI. Section VII evaluates the performance of the proposed scheme by comparing it with other schemes available in the literature. Finally, Section VIII provides our conclusions.

II. System Model

We consider a SISO OFDM system using QPSK modulation, where QPSK symbols are grouped in blocks of length N, where N is the number of used subcarriers. The resulting blocks are then processed by an IDFT to obtain the time-domain samples to be transmitted serially through the $\mathcal{L}$ tap frequency selective channel. To avoid intersymbol interference (ISI) the blocks are preceded by a cyclic prefix (CP), which should be longer than the channel impulse response $\mathcal{L}$. The OFDM symbols are further organized in data frames of M symbols. P_t and P_f pilot symbols are placed uniformly in time and frequency respectively within data frames according to [31].

The received samples after passing through the noisy channel, CP removal, and DFT processing can be written in vector notation as

$$\mathbf{r} = \mathbf{F}\boldsymbol{\mathcal{H}}\mathbf{F}^H\mathbf{s} + \mathbf{F}\tilde{\mathbf{w}} = \mathbf{H}\mathbf{s} + \mathbf{w}, \tag{1}$$

where the vectors $\mathbf{s} \in \mathcal{C}^{N\times 1}$ and $\mathbf{r} \in \mathcal{C}^{N\times 1}$ contain transmitted and received symbol samples respectively, $\mathbf{F}$ is the DFT matrix with elements $[\mathbf{F}]_{k,l} = (1/\sqrt{N})e^{-j2\pi kl/N}$, $\boldsymbol{\mathcal{H}}$ is the time domain channel matrix affecting the current symbol, and $\mathbf{H} = \mathbf{F}\boldsymbol{\mathcal{H}}\mathbf{F}^H$ is the channel matrix in frequency domain. Finally, $\mathbf{w} \in \mathcal{C}^{N\times 1}$ is a vector of complex AWGN samples. In this paper we will assume that the channel remains static for a whole symbol but is allowed to vary from symbol to symbol such that matrix $\mathbf{H}$ becomes diagonal for each OFDM symbol, with diagonal elements given by vector $\mathbf{h}[m] = [h_0[m], \ldots h_{N-1}[m]]^T$ for symbol time m.

This assumption is reasonable for the considered channel prediction application as the system parameters and mobile speeds of interest in practical implementations result indeed in an almost diagonal structure for $\mathbf{H}$. Nevertheless, if ICI must be taken into consideration, ICI equalizers like those presented in [32] and [33] can be used in conjunction with the estimation/prediction schemes presented here with only a minor modification in the pilot signaling.

We can thus rewrite (1) in terms of the diagonal elements of $\mathbf{H}$ for each subcarrier $h_k, (k = 0, \ldots, N-1)$ at symbol time m $(m = 0, \ldots, M-1)$ as

$$r_k[m] = h_k[m]s_k[m] + w_k[m]. \tag{2}$$

III. Recursive BEM Design

In this section we model the dynamics of the time evolution of the channel with a small set of parameters that can be extracted from the received samples in (2). In the following, the main design steps involved are described.

A. Channel Time Evolution Basics

Let us consider the channel variation on the kth OFDM subcarrier of (2) during a data frame of M OFDM symbols. This can be denoted by arranging the values of $h_k[m]$ in (2) for $m = 0, \ldots, M-1$ in a vector as $\mathbf{h}_k = [h_k[0], \ldots, h_k[M-1]]^T$. As we focus for now on only one subcarrier, we drop the subscript k to simplify the notation.

Vector $\mathbf{h}$ can be described by means of an adequate linear transform as $\mathbf{h} = \mathbf{T}^H\boldsymbol{\gamma}$, where $\mathbf{T}$ is an $(M \times M)$ orthonormal transformation matrix and $\boldsymbol{\gamma} = [\gamma[0], \ldots, \gamma[M-1]]^T$ is an $(M \times 1)$ vector containing the transformed description coefficients on the current data frame. It is known [3] that with an appropriate choice of the transformation matrix $\mathbf{T}$, $\mathbf{h}$ can be accurately fitted by a BEM with dimension reduced to G $(G \ll M)$ such that

$$\hat{\mathbf{h}} = \bar{\mathbf{T}}^H\bar{\boldsymbol{\gamma}}, \tag{3}$$

where $\hat{\mathbf{h}}$ is the vector with the approximated channel values for current data frame, $\bar{\mathbf{T}}$ is an $(G \times M)$ matrix built from the first G rows of $\mathbf{T}$, and $\bar{\boldsymbol{\gamma}} = [\gamma[0], \ldots, \gamma[G-1]]^T$ is the vector with the truncated basis expansion coefficients. The number of basis functions G required for a good fit of $\mathbf{h}$ depends on the energy compaction characteristic of the particular transformation used [3].

Using (3) we have that the expected value of the energy associated to the realizations of $\mathbf{h}$ is given by

$$E\left\{\sum_{m=0}^{M-1}|h[m]|^2\right\} = E\left\{\sum_{m=0}^{M-1}|\hat{h}[m]|^2\right\} + \sigma_e^2, \tag{4}$$

where the first term on the right-hand side represents the energy of $\mathbf{h}$ which is captured by the BEM of (3), and the second term is the residual energy from the coefficients of $\boldsymbol{\gamma}$ discarded in (3).

B. DCT Approximation

It has been shown in [22] that the DFT has worse energy compression than DCT for Jakes Doppler spectrum. In [5] it was also shown that DPSS are optimal for ideal low-pass Doppler spectrum. Although the performance, in terms of MSE, of DPSS-BEM is slightly better than that of DCT-BEM, the basis functions of DPSS-BEM are not well suited for a low order recursive implementation. On the other hand, the sinusoidal basis functions of DCT-BEM can be efficiently approximated with low order and numerically stable recursive filters taken from the well known theory of notch filters [34] as will be shown in the following subsection.

The classical approach for selecting the value of G when constructing a BEM is to set $G = \lceil 2\pi\nu_d M \rceil + G'$, where ν_d refers to normalized Doppler shift, and G' is a bandwidth margin chosen to compensate for the spectral leakage introduced by the BEM representation. Excessively small values of G' degrade the MSE performance of the BEM, because the discarded spectral leakage can be significant. On the other hand, if G' is set too large, the included low energy BEM coefficients would also degrade the performance as they are more sensitive to noise.

Based on the energy compaction property of DCT, a criterion for selecting the appropriate value of G, which we use here, was

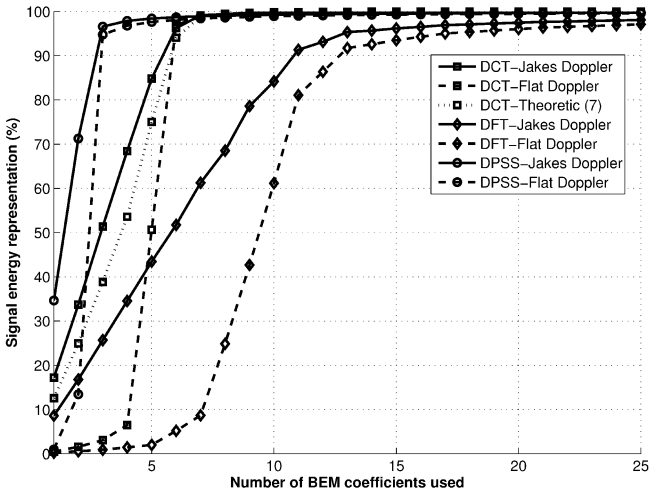

Fig. 1. Comparison of the energy compactation for different BEMs. Results are shown for Jakes and Flat Doppler models with a maximum normalized Doppler shift $\nu_d = 0.01$. The block length is set to 256 OFDM symbols and results are averaged over 100 channel realizations. The theoretical performance evaluated for DCT using (7) for Jakes Doppler model is also shown for reference.

proposed in [22]. The criterion is based on the characterization of the spectral leakage introduced by DCT when used to represent the channel Doppler. The value of G is selected according to

$$G = \arg\min_{\bar{G}} \left| 1 - \frac{1}{(M-\bar{G}) L_{\mathrm{DCT}}(\bar{G})} \right|, \tag{5}$$

where L_{DCT} is the spectral leakage associated to trial value $\bar{G}$. That is,

$$L_{\mathrm{DCT}}(\bar{G}) = \frac{1}{\sigma^2_{\mathbf{h}}} \sum_{m=\bar{G}}^{M-1} \sigma^2_{\mathrm{DCT}}[m], \tag{6}$$

where $\sigma^2_{\mathbf{h}}$ is the energy of $\mathbf{h}$ and $\sigma^2_{\mathrm{DCT}}[m]$ the variance associated to the mth coefficient of the DCT representation of the channel Doppler, which can be written in terms of the autocorrelation function of the channel $R_{\mathbf{hh}}(i)$ as

$$\sigma^2_{\mathrm{DCT}}[m] = \sigma^2_{\mathbf{h}} A^2(m) \sum_{i=0}^{M-1} \sum_{j=0}^{M-1} R_{\mathbf{hh}}(i-j) \times \cos\left(\frac{\pi \left(i+\frac{1}{2}\right) m}{M} \right) \cos\left(\frac{\pi \left(j+\frac{1}{2}\right) m}{M} \right), \tag{7}$$

where $A(m) = 1/\sqrt{M}$ for $m = 0$ and $\sqrt{2/M}$ for $1 \le m \le M-1$. Fig. 1 plots the channel energy representation [the first term on the right hand side of (4)] as a function of the truncation order for DCT, DFT, and DPSS BEMs. This figure illustrates the truncated BEM modeling error showing that for a modeling error below 2%, DCT-BEM and DPSS-BEM require roughly the same number of basis functions. On the other hand, DFT-BEM, which has a poor compactation characteristic, requires many more basis functions.

Another frequently used approach for model order selection, typically used in SOS based estimators [35] is based on the minimum description length (MDL) method. MDL criterion is similar in spirit to the criterion proposed in [22], while being more general and better suited for SOS estimators where all parameters of the associated SOS-BEM are determined from a sample estimation of the autocorrelation function of the channel [35]. Different from DCT-BEM where the basis function frequencies are known, SOS-BEM relies on the estimation of the frequencies of the sinusoidal basis functions through spectral estimation techniques. In that case, the criterion used here and derived specifically for DCT-BEM (where the sinusoidal frequencies are known) does not apply.

C. Recursive BEM

Considering DCT in (3), the elements of matrix $\bar{\mathbf{T}}$ can be written for $i = 0 \ldots G-1$ and $m = 0 \ldots M-1$ as

$$[\bar{\mathbf{T}}]_{i,m} = A(m) \cos\left(\frac{\pi \left(i+\frac{1}{2}\right) m}{M} \right), \tag{8}$$

such that $\hat{h}_{(\mathrm{DCT})}[m]$ is given by the linear combination of the corresponding DCT basis functions. These basis are cosine functions at harmonic frequencies, defined by the frame length M and the corresponding basis function index i. Each row of matrix $\bar{\mathbf{T}}$ in (8) can be interpreted as the impulse response of an ideal bandpass filter centered at the corresponding cosine frequency. Based on [36], the corresponding transfer function of each DCT row $0 \le i \le G-1$ is given by

$$H_{\mathrm{DCT}_i}(e^{j\omega}) = c_i \frac{(-1)^i - (-1)^i e^{-j\omega} - e^{-j\omega M} + e^{-j\omega(M+1)}}{1 + 2\cos(i\pi/M) e^{-j\omega} + e^{-j2\omega}}, \tag{9}$$

where notation H_{DCT_i} indicates the filter that outputs $\hat{h}_{(\mathrm{DCT})_i}[m]$ (the ith DCT component of the channel) when the input is given by the channel sequence $h[m]$, and where $c_i = A(i)\cos((\pi i)/(2M))$. Filters in (9) can be used to obtain $\hat{h}_{(\mathrm{DCT})}[m]$ in (3) recursively by extracting the DCT frequency representation components (8) of $h[m]$ (weighted by their corresponding γ_i coefficient). Then the time domain channel evolution representation in terms of DCT can be expressed, using the difference equation notation of H_{DCT} for a compact description, as the sum of the output of these filters when fed with the channel sequence as

$$\hat{h}_{(\mathrm{DCT})}[m] = H_{\mathrm{DCT}}(q^{-1}) h[m] = \sum_{i=0}^{G-1} H_{\mathrm{DCT}_i}(q^{-1}) h[m], \tag{10}$$

being $H_{\mathrm{DCT}}(q^{-1})$ and $H_{\mathrm{DCT}_i}(q^{-1})$ the difference equation representation of the DCT filter bank and the DCT components filters of (9) respectively.

Using a low complexity recursive filter bank to approximate each of these rows we can obtain an estimate of $h[m]$ from its

noisy samples. The lattice realization is known to be orthogonal and have very good numerical behavior for the implementation of narrow passband filters [37]. Thus, the proposed model for $\hat{h}_{(F)}[m]$ is based on the approximation of the FIR filter described by (10), by a bank of narrow passband filters such that

$$\hat{h}_{(F)}[m] = H_F(q^{-1})h[m] = \sum_{i=0}^{G-1} \beta_i H_{F_i}(q^{-1})h[m], \quad (11)$$

where

$$H_F(e^{j\omega}) = \beta_0 \frac{0.5(1-s_{20})(1+e^{-j2\omega})}{1-s_{20}e^{-j2\omega}} + \sum_{i=1}^{G-1} \beta_i \frac{0.5(1-s_{2i})(1-e^{-j2\omega})}{1+(s_{2i}+1)s_{1i}e^{-j\omega}+s_{2i}e^{-j2\omega}}, \quad (12)$$

and $s_{1i} = \sin\theta_{1i} = -\cos((\pi i)/(M))$ is the lattice parameter defining the central frequency, $s_{2i} = \sin\theta_{2i}$ $(0 < s_{2i} < 1)$ is related to the 3 dB bandwidth B_i of each narrow band filter by $\sin\theta_{2i} = [(1 - \tan(B_i/2))/(1 + \tan(B_i/2))]$ and β_i are real valued scaling coefficients. Except for the first filter, the filter bank is based on the normalized allpass realization [37].

Remarks:

- It is worth noting that (9) has M zeros and two poles. The zeros are located on the unit circle equispaced in $2i\pi/M$ starting at frequency $i\pi/M$, and the poles, also on the unit circle, are located at frequencies $\pm i\pi/M$. After the pole/zero cancellations, the frequency response obtains its maxima at $\pm i\pi/M$.
- The main objective to replace (10) (FIR) with the *recursive* (IIR) realization of (11) is to obtain a low complexity estimator-predictor as discussed in the next sections.
- Since basis function of the proposed realization is an approximation of the DCT basis, its energy compaction properties are also suitable for Doppler representation. To control the approximation error to the corresponding DCT of (9), the proposed realization has two tuning parameters, s_{2i} and β_i. The characteristics of this approximation error and its relation to the tuning parameters are discussed in the next subsection.

D. DCT—Filter Bank Approximation Error

We conclude this section by studying the characteristics of the approximation error involved between (10) and (11). To that purpose, disregarding measurement noise for this analysis, and assuming that the Doppler power spectral density of $h[m]$, $S_D(e^{j\omega})$ is perfectly represented by the DCT basis, we obtain the scaling coefficients β_i in (12) that minimize the mean-square error (MSE) representation when using (11).

The mean-square error with respect to the reconstructed sequence $\hat{h}_{(F)}[m]$ at the proposed filter bank output can be expressed as

$$\xi = E\left\{|e[m]|^2\right\} = E\left\{\left|h[m] - \hat{h}_{(F)}[m]\right|^2\right\}, \quad (13)$$

where $h[m] = H^*_{\mathrm{DCT}}(q^{-1})\hat{h}_{(\mathrm{DCT})}[m]$ giving $\hat{h}_{(F)}[m] = H_F(q^{-1})H^*_{\mathrm{DCT}}(q^{-1})\hat{h}_{(\mathrm{DCT})}[m]$, with $H^*_{\mathrm{DCT}}(e^{j\omega})$ the frequency response of the inverse DCT transfer function. If the channel Doppler spectrum is bandlimited to a normalized Doppler frequency $\nu = \nu_d$, (13) can be written as

$$\xi = \int_{-\nu_d}^{\nu_d} S_{\mathrm{MSE}}(e^{j\omega})d\omega = \int_{-\nu_d}^{\nu_d} \left|1 - H_F(e^{j\omega})H^*_{\mathrm{DCT}}(e^{j\omega})\right|^2 S_D(e^{j\omega})\,d\omega. \quad (14)$$

By defining

$$\alpha_i = \int_{-\nu_d}^{\nu_d} \mathrm{Re}\left\{H_{F_i}(e^{j\omega})H^*_{\mathrm{DCT}}(e^{j\omega})\right\}S_D(e^{j\omega})\,d\omega,$$

$$\phi_{i,l} = \int_{-\nu_d}^{\nu_d} \mathrm{Re}\left\{H_{F_i}(e^{j\omega})H^*_{F_l}(e^{j\omega})\right\}\left|H_{\mathrm{DCT}}(e^{j\omega})\right|^2 \times S_D(e^{j\omega})\,d\omega,$$

for $0 \le i, l \le G-1$, (14) can be rewritten as

$$\xi = d - 2\boldsymbol{\beta}^T\boldsymbol{\alpha} + \boldsymbol{\beta}^T\boldsymbol{\Phi}\boldsymbol{\beta}, \quad (15)$$

where $d = \int_{-\nu_d}^{\nu_d} S_D(e^{j\omega})\,d\omega$, $\boldsymbol{\alpha} = [\alpha_0, \ldots, \alpha_{G-1}]^T$, $\boldsymbol{\Phi}$ is a $G \times G$ matrix formed by $\phi_{i,l}$ and $\boldsymbol{\beta} = [\beta_0, \ldots, \beta_{G-1}]^T$. As can be easily concluded, the MSE is quadratic in $\boldsymbol{\beta}$, and the optimum is given by

$$\boldsymbol{\beta} = \boldsymbol{\Phi}^{-1}\boldsymbol{\alpha}. \quad (16)$$

Furthermore, the minimum MSE is then given by

$$\xi_{\min} = d - \boldsymbol{\alpha}^T\boldsymbol{\Phi}^{-1}\boldsymbol{\alpha}. \quad (17)$$

Remarks:

- If we assume, to assess the filter bank approximation error, that the channel Doppler power spectral density $S_D(e^{j\omega})$ can be perfectly represented by the DCT, the MSE so defined is only due to the mismatch between the filter bank and the DCT representations.
- Note that using $\beta_i H_{F_i}(e^{j\omega}) = H_{\mathrm{DCT}_i}(e^{j\omega})$ in (15), the residual MSE $\xi_o \le \xi_{\min}$ verifies $\xi_o = \int_{-\nu}^{\nu}(1 - |H_{\mathrm{DCT}}(e^{j\omega})|^2)^2 S_D(e^{j\omega})\,d\omega$, as required in (14).
- Clearly, (17) gives a lower bound to the mean square approximation error between the proposed Doppler representation and the DCT.

Figs. 2 and 3 illustrate $S_{\mathrm{MSE}}(e^{j\omega})$ of (14) for Jakes and Flat Doppler spectrum, respectively. In both figures, the filter bank coefficients β_i are either optimized using (16) or just set all equal to one (to simplify the representation). $S_{\mathrm{MSE}}(e^{j\omega})$ is plotted for a typical value of $s_{2i} = 0.9978$ (set equal for all passband filters in the filter bank) for both Doppler models. Since s_{2i} determines the bandwidth of the filters, it also controls the overlap among them. When using the optimum β_i, this overlap among filters is included in the design of the filter bank thus leading to an improvement on the approximation error, as can be seen in Figs. 2 and 3.

Note that $S_{\mathrm{MSE}}(e^{j\omega})$ in Fig. 3 is not perfectly uniform over the Doppler frequency band. This is because the passband filters' frequency responses are not symmetrical around their central frequencies leading to more overlapping to higher than to lower frequencies. This makes $S_{\mathrm{MSE}}(e^{j\omega})$ to be lower for

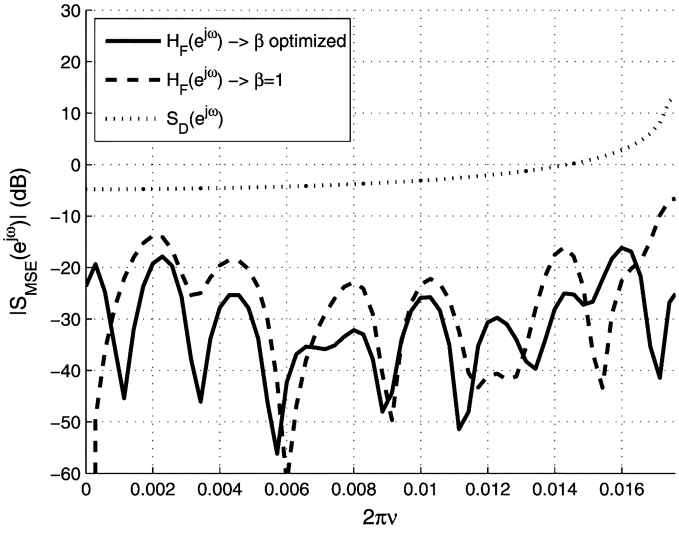

Fig. 2. $S_{\mathrm{MSE}}(e^{j\omega})$ for Jakes Doppler model with β_i optimized and $\beta_i = 1$ and parameter $s_{2i} = s_2$ set to a typical value. Equation (14) gives $\xi = -28.25$dB for optimized β_i and $\xi = -21.78$ dB for $\beta_i = 1$.

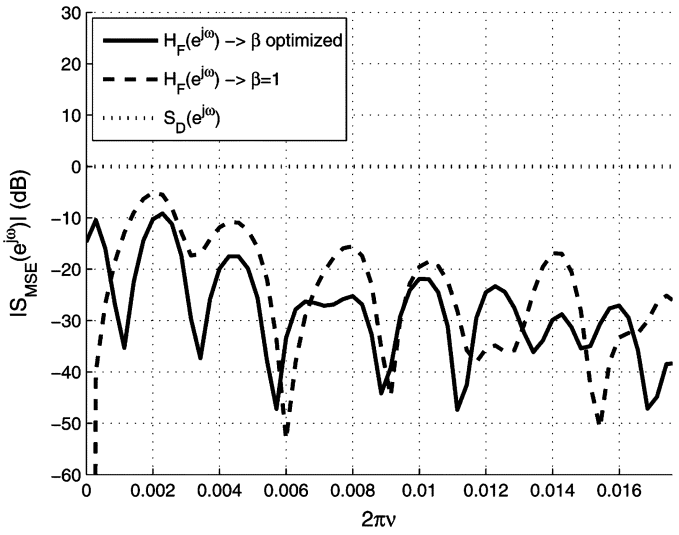

Fig. 3. $S_{\mathrm{MSE}}(e^{j\omega})$ for Flat Doppler model with β_i optimized and $\beta_i = 1$ and parameter $s_{2i} = s_2$ set to a typical value. Equation (14) gives $\xi = -24.70$ dB for optimized β_i and $\xi = -19.85$ dB for $\beta_i = 1$.

higher frequencies as the notches between different passbands are smother because of the higher overlap.

Fig. 2 (Jakes Doppler), shows that $S_{\mathrm{MSE}}(e^{j\omega})$ increases around the frequency where the Doppler has its typical peak. As this peak does not coincide with the central frequency of any passband filter but lies between two of them, the notch between the passbands leads to this increase in $S_{\mathrm{MSE}}(e^{j\omega})$.

Formally, if *a priori* information about the Doppler shape is available, s_{2i} can be tuned to better fit its characteristic. Fig. 4 illustrates this tuning for Jakes Doppler model, where the passband filters bandwidth is set slightly broader for the high frequency filters to better capture the spectrum peak present in Jakes model. Comparing Figs. 2 and 4 it can be seen that the tunning of s_{2i} effectively reduces the error around the Doppler peak at ν_d. When s_{2i} is tuned according to the Doppler model, the plot for $S_{\mathrm{MSE}}(e^{j\omega})$ for $\beta = 1$ is seen to be higher towards ν_d as compared to the equal s_{2i} case of Fig. 2. This happens because

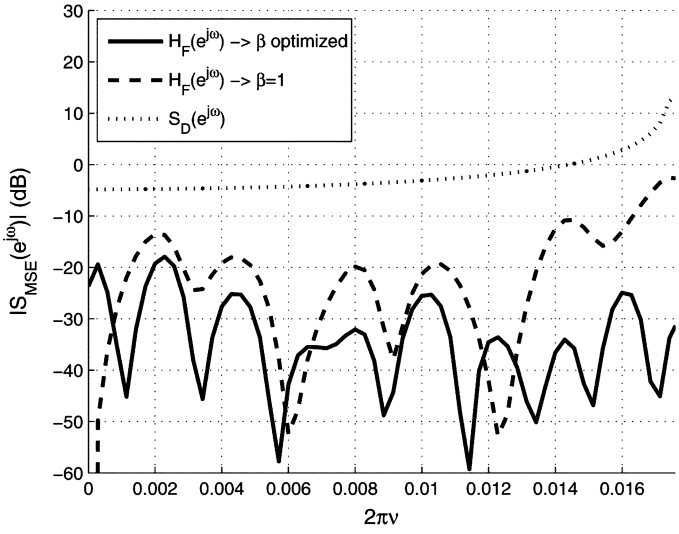

Fig. 4. $S_{\mathrm{MSE}}(e^{j\omega})$ for Jakes Doppler model with β_i optimized and $\beta_i = 1$ and parameter s_{2i} tuned according to the Doppler Model. Equation (14) gives $\xi = -30.65$ dB for optimized β_i and $\xi = -16.67$ dB for $\beta_i = 1$.

the increase in bandwidth in the higher frequency passband filters results in more overlapping among filters in that frequency region. Without the β_i to scale this extra overlap, $S_{\mathrm{MSE}}(e^{j\omega})$ increases in that region.

Figs. 2 to 4 are calculated for a maximum normalized Doppler frequency of $\nu_d = 2.8 \times 10^{-3}$, a DCT size of $M = 1100$ and $G = 8$ chosen according to (5).

IV. Channel Estimator

By defining $\mathbf{x}_i[m]$, $0 \le i \le G-1$, the (2×1) state vector for each passband filter, we can express the filter bank structure for the recursive BEM implementation in state space form as

$$\begin{aligned} \mathbf{x}_i[m+1] &= \mathbf{A}_i \mathbf{x}_i[m] + \mathbf{b}_i h[m] \\ \hat{h}_{i(F)}[m] &= \mathbf{c}_i \mathbf{x}_i[m] + d_i h[m] \\ \hat{h}_{(F)}[m] &= \sum_{i=0}^{G-1} \beta_i \hat{h}_{i(F)}[m], \end{aligned} \tag{18}$$

where, for $i = 0$

$$\mathbf{A}_0 = \begin{bmatrix} 0 & s_{20} \\ 1 & 0 \end{bmatrix} \quad \mathbf{b}_0 = \begin{bmatrix} 1 \\ 0 \end{bmatrix}$$
$$\mathbf{c}_0 = \begin{bmatrix} 0 & 1 - s_{20} \end{bmatrix} \quad d_i = 0.5(1 - s_{20}),$$

and for $1 \le i \le G-1$, defining $c_{ji} = \sqrt{1 - s_{ji}^2}$,

$$\mathbf{A}_i = \begin{bmatrix} -s_{1i} & -s_{2i}c_{1i} \\ c_{1i} & -s_{2i}s_{1i} \end{bmatrix} \quad \mathbf{b}_i = \begin{bmatrix} c_{2i}c_{1i} \\ c_{2i}s_{1i} \end{bmatrix}$$
$$\mathbf{c}_i = \begin{bmatrix} 0 & -c_{2i} \end{bmatrix} \quad d_i = 1 - s_{2i}.$$

From (2) we have that the input signal to the filter bank is not $h[m]$ but its equalized version given by $\bar{h}[m] = r[m]/\hat{s}[m] + w[m]/\hat{s}[m]$, where $\hat{s}[m]$ is either a known pilot symbol or an estimate of the transmitted symbol based on the previous channel estimate. Then, as $w[m]$ is assumed to be AWGN, the optimum algorithm for estimating $h[m]$ is a set of G scalar Kalman filters for the filter bank of (18).

In order to obtain the estimator, the Kalman filter gain for each narrow passband filter of (18) is given by the solution of the following Riccati equation:

$$\mathbf{P}_i = \mathbf{A}_i \left(\mathbf{P}_i - \mathbf{P}_i \mathbf{c}_i^T \left(\mathbf{c}_i \mathbf{P}_i \mathbf{c}_i^T + d_i^2 \sigma_h^2 \right)^{-1} \mathbf{c}_i \mathbf{P}_i \right) \mathbf{A}_i^T + \mathbf{b}_i \sigma_h^2 \mathbf{b}_i^T, \quad (19)$$

that allows to obtain the steady-state Kalman gain for filter i given by

$$\mathbf{K}_i = \mathbf{P}_i \mathbf{c}_i^T \left(\mathbf{c}_i \mathbf{P}_i \mathbf{c}_i^T + d_i^2 \sigma_h^2 \right)^{-1}. \quad (20)$$

More importantly, and different to the Kalman formulations presented in [9], [29], the matrices in (18) describing the filter bank are time invariant since the BEM is kept fixed for the whole transmission. Thus, the Kalman formulation will have a steady-state solution avoiding most of the complexity of the Kalman filter as the steady-state gains $\mathbf{K}_i$ can be calculated offline. Moreover, in view of [38, Th. 6.3, Ch. 6], the steady-state estimate and the optimal estimate are exponentially close to each other. The resulting limiting Kalman filter is given by

$$\begin{aligned} e[m] &= r[m] - \hat{s}[m] \hat{h}_{(K)}[m-1] \\ \mathbf{x}_i[m] &= \mathbf{A}_i \mathbf{x}_i[m-1] + \mathbf{K}_i \hat{s}^*[m] e[m] \\ \hat{h}_{i(K)}[m] &= \mathbf{c}_i \mathbf{x}_i[m] \\ \hat{h}_{(K)}[m] &= \sum_{i=0}^{G-1} \beta_i \hat{h}_{i(K)}[m]. \end{aligned} \quad (21)$$

We finally note that the solution of the Riccati equation of (19) can be obtained using the algorithms described in [39]. The issues related to the numerical condition of the solution process and balancing to improve the condition are discussed therein, and low complexity iterative refinement procedures for the solution are provided. These iterative methods have the advantage of improving the accuracy of computed solutions in case of ill conditioned equations [39].

V. Channel Predictor

The structure presented in Section IV, given by (21), is useful to obtain an ARMA-model-based long-range predictor (LRP) [13], [40]. To that purpose, and considering that the channel estimated vector is highly oversampled, a properly frequency scaled version of the filter bank of (18) is fed with channel estimates $\hat{h}_{(K)}[m]$ decimated by a factor T. Since relative frequencies of the decimated input are T times higher, frequency scaling of the filter bank is necessary to compensate for the decimation.

Factor T is chosen such that the decimated channel estimates are slightly oversampled. The resulting prediction range becomes $T \times L$. where L is the extrapolation factor of the Kalman filter predictor. As result, the limiting Kalman filter predictor is given by

$$\begin{aligned} e^p[m+\ell] &= \hat{h}_{(K)}[m+\ell-T] - \hat{h}^p[m+\ell-T] \\ \mathbf{x}_{i\ell}^p[m+\ell] &= (\mathbf{A}_i^p)^L \mathbf{x}_{i\ell}^p[m+\ell-TL] + \mathbf{K}_i^p e^p[m+\ell] \\ \hat{h}_i^p[m+\ell] &= \mathbf{c}_i^p \mathbf{x}_{i\ell}^p[m+\ell] \end{aligned}$$

$$\hat{h}^p[m+\ell+T(L-1)] = \sum_{i=0}^{G-1} \beta_i \hat{h}_i^p[m+\ell], \quad (22)$$

where $\ell = 0, \ldots, (T \times L) - 1$ are the state vector samples used at each iteration, $\mathbf{x}_{i\ell}^p$ is the predictor state vector (analogous to $\mathbf{x}_i$ in (21)), $\mathbf{A}_i^p$ and $\mathbf{c}_i^p$ are the transition matrix and output vector of the passband filters scaled up in frequency by T, and given for $i = 0$ by

$$\mathbf{A}_0^p = \begin{bmatrix} 0 & s_{20}^p \\ 1 & 0 \end{bmatrix} \quad \mathbf{c}_0 = [\,0 \quad 1 - s_{20}^p\,],$$

and for $1 \leq i \leq G-1$ by

$$\mathbf{A}_i^p = \begin{bmatrix} -s_{1i}^p & -s_{2i}^p c_{1i}^p \\ c_{1i}^p & -s_{2i} s_{1i} \end{bmatrix} \quad \mathbf{c}_i^p = [\,0 \quad -c_{2i}^p\,],$$

where $s_{1i}^p = -\cos((\pi i T)/(M))$ is the lattice parameter defining the scaled up in frequency narrowband filter central frequency, s_{2i}^p $(0 < s_{2i}^p < 1)$ sets the selectivity of the passband filters, and $c_{ji}^p = \sqrt{1 - {s_{ji}^p}^2}$. Finally $\mathbf{K}_i^p$ can be obtained (offline) by solving

$$\mathbf{P}_i = \mathbf{A}_i^p \left(\mathbf{P}_i - \mathbf{P}_i \mathbf{c}_i^{pT} \left(\mathbf{c}_i^p \mathbf{P}_i \mathbf{c}_i^{pT} + d_i^{p2} \sigma_h^2 \right)^{-1} \mathbf{c}_i^p \mathbf{P}_i \right) \mathbf{A}_i^{pT} + \mathbf{b}_i^p \sigma_h^2 \mathbf{b}_i^{pT}, \quad (23)$$

that allows to obtain the steady-state Kalman gain for filter i given by

$$\mathbf{K}_i^p = \mathbf{P}_i \mathbf{c}_i^{pT} \left(\mathbf{c}_i^p \mathbf{P}_i \mathbf{c}_i^{pT} + d_i^{p2} \sigma_h^2 \right)^{-1}. \quad (24)$$

A block diagram of the estimator-predictor proposed is depicted in Fig. 5.

In the conventional LRP [40] a specific model for the Doppler spectrum is assumed (AR Jakes approximation in general), which is not the case in practical channels. This leads to a modeling error floor that reduces the prediction range. This is not the case in the proposed structure due to the BEM formulation. The proposed predictor can also be interpreted as a low complexity variation of a sum of sinusoids (SOS) predictor ([17] and references therein) as it is based on the prediction of approximated superimposed sinusoidal components. Different to SOS predictors, the proposed BEM does not requires estimation of the frequencies associated with individual sinusoids. Thus, complexity of the approximated DCT BEM predictor is significantly reduced compared to SOS predictors.

It remains to extend the developed channel estimator/predictor scheme for frequency selective channels. According to [31, Th. 1], an estimate of $\mathrm{diag}(\mathbf{H})$ in (1) for each symbol can be obtained by using $P_f \geq \mathcal{L}$ pilot subcarriers that are equispaced within the OFDM symbol. We can thus design a selective channel predictor by using the flat fading estimator and predictor proposed on each of these P_f pilot subcarriers. The channel coefficients for all subcarriers can be then obtained using DFT interpolation in frequency.

An alternative to this last step is to use truncated DCT interpolation as in [41] (see also [18]–[20], [26]). Although in the

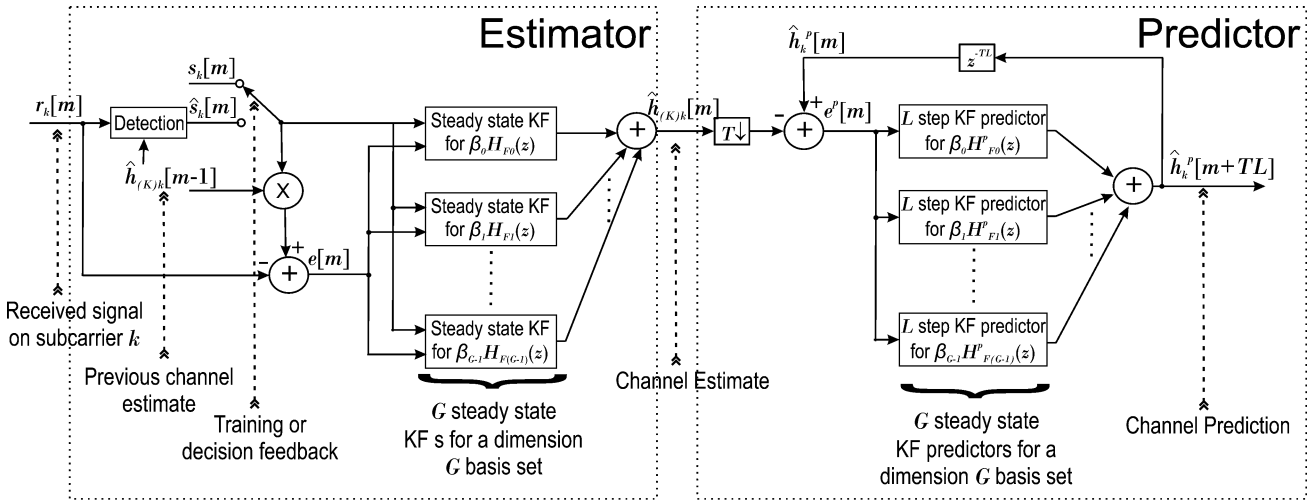

Fig. 5. Estimator-predictor block diagram for each channel coefficient.

case of an ideal FIR channel, DFT gives the lowest truncation order (length of the FIR channel) and no interpolation error, in practical channel realizations the channel delays are not multiples of the sampling time [42]. In this general case, energy dispersion over DFT coefficients is larger than for DCT. Hence DCT renders a lower computational cost than DFT, because the better energy compactation property of DCT allows the DCT interpolation matrix to be truncated to G_f rows similarly to (3). Further, the aliasing effect in case of nonsample spaced path delays is significantly mitigated in the DCT approach [18], [19], [25].

VI. Complexity Analysis

We consider the computational complexity of the proposed channel estimator/predictor assuming operation over a frequency selective fading channel.

The complexity involved in the solution of the Riccati equations of the proposed scheme can be high, because of the iterative refinement of the solution [39]. However, the limiting Kalman gains for (21) and (22) can be computed offline, and therefore the corresponding computational cost is not considered in this analysis. Equation (21) requires $2 + 15G$ complex operations to output each channel estimate while (22) requires $T \times L \times (1+25G)$ complex operations to output $T \times L$ symbol sampled channel predictions. The complexity for the frequency selective scenario would be P_f times this computational load, for the estimation/prediction over the P_f pilot subcarriers (for a maximum of P_f channel taps), plus the computational load involved in the frequency interpolation operation to obtain the channel prediction for all subcarriers.

As no model parameters need to be estimated, the complexity corresponding to the iteration of both limiting Kalman filters results in a complexity of $\mathcal{O}(G)$ times the complexity of the LMS algorithm for each of the P_f filter banks used. Moreover, as G_f $(\leq P_f)$ is usually much lower than N the overall complexity is small. The interpolation task has a computational complexity in the order of $\mathcal{O}(G_f \log_2 N)$ for a truncated DCT of dimension G_f, being G_f upper bounded by P_f.

Table I summarizes the complexity analysis for the proposed recursive-BEM-LR channel predictor. For comparison purposes the table includes also a low complexity RLS based MMSE-LR channel predictor [43] and a reduced complexity ESPRIT based SOS channel predictor [35] both available in the literature. For the predictor of [43], $\mathcal{M}$ is the amount of memory used by the predictor. For the SOS predictor of [35], P_t plays a similar role as parameter G in our design and determines the Doppler frequency resolution of the estimator/predictor. P_t together with P_f determine the time-frequency grid over which the algorithm calculates the estimated number of channel taps $\hat{\mathcal{L}}$ (upper bounded by P_f). R and $\bar{R}$ stand for the maximum and average number of rays per channel tap respectively and are upper bounded by the value of P_t. For the same system parameters the predictor of [35] is considerably more computationally expensive than the other two since R and $\bar{R}$ are comparable in magnitude to G and $\mathcal{M}$ and the initialization step requires several data frames. It is worth noting that the RLS-MMSE initialization complexity is not detailed in [43]. This predictor is initialized as described in the last two equations of [43, Sec. IV-B], whose computational cost was evaluated for Table I as the computational cost of the coefficient update operation.

TABLE I
Computational Complexity Comparison

	Initialization	Pred. Iteration	Coeff. Update
R-BEM proposed estim./pred.	-	$\mathcal{O}(P_f G + G_f \log_2 N)$	-
Low compl. RLS-MMSE pred. [43]	$\mathcal{O}(P_f \mathcal{M}^2)$	$\mathcal{O}(P_f \mathcal{M} + N \log_2 N)$	$\mathcal{O}(P_f \mathcal{M}^2)$
Red. compl. ESPRIT pred. [35]	$\mathcal{O}(P_f^3 + \hat{\mathcal{L}} P_t^3)$	$\mathcal{O}(N\hat{\mathcal{L}} + \bar{R})$	$\mathcal{O}(P_f^2 + P_t R)$

VII. Simulations

An appropriate measure for evaluating channel prediction performance is the normalized mean square error (NMSE) defined by

$$\mathbf{NMSE} = \frac{\mathrm{E}\left\{|h[m] - \hat{h}^p[m]|^2\right\}}{\mathrm{E}\left\{|h[m]|^2\right\}}. \tag{25}$$

The performance of the proposed tecursive-BEM (R-BEM) LRP is evaluated in terms of the NMSE and compared with a MMSE LRP [13] and ESPRIT based SOS predictor [44]. The performance measure of interest in this work is the length of the achievable prediction horizon, subject to a certain NMSE constraint.

In [43] it was shown that a reduced complexity MMSE predictor based on RLS algorithm can attain almost the same performance as the MMSE channel predictor of [13]. Thus, the comparison with the conventional MMSE LRP of [13] serves as the best performance bound for the low complexity predictor of [43]. We also compare our predictor with the ESPRIT based SOS predictor of [44]. In [35], the authors present a reduced complexity version of [44] so that comparison with [44] can be used as the best performance bound of the reduced complexity version presented in [35].

To normalize the prediction range with respect to mobile velocity, we use the spatial unit wavelength λ, where a prediction of τ seconds ahead corresponds to $\lambda = f_{dm}\tau$ wavelengths, being f_{dm} the maximum Doppler shift [17]. An NMSE threshold of -20 dB as proposed in [45] is used to determine the limit of prediction horizon. We consider an OFDM system operating at a carrier frequency $f_C = 2$ GHz with 10.24 MHz bandwidth and 20 KHz subcarrier spacing. The number of subcarriers is set to $N = 512$ and the length of the cyclic prefix is 27. The frame length is set to $M = 22$ OFDM symbols, equivalent to 2 ms. The system uses 5% pilot ratio, distributed uniformly in time and in frequency, using $\lfloor 2.8\mathcal{L} \rfloor$ pilots in frequency, and the number of DCT basis functions for frequency domain channel interpolation is set to $G_f = \lfloor 1.2\mathcal{L} \rfloor = 32$. The parameters for the proposed filter bank realization are based on 12 frames such that $s_{1i} = -\cos((\pi i)/(M_v))$, $M_v = 12M$. The value of G was chosen from the maximum normalized Doppler shift ν_{dm} according to (5) ($G = 6$ for mobile speed of 30 km/h). Also, a simplified form of the filter bank is used, i.e., $\beta_i = 1$ (not optimized) and equal s_{2i}, $0 \leq i \leq G-1$. For realistic results, we consider a wireless fading channel following the ITU-Vehicular A specification, which results in a 27-tap frequency selective channel for the given system parameters. All channel taps vary in time following the same Doppler spectrum. Different Doppler spectrums were evaluated to show the robustness of the proposed prediction scheme to the Doppler shape. All the simulation results were obtained by averaging over 11000 OFDM symbols equivalent to 55 data frames.

Fig. 6 shows the NMSE as a function of the prediction range for the R-BEM LRP, the MMSE LRP of [13] with a memory of 10 samples and the ESPRIT based SOS predictor of [44]. The -20 dB threshold is also depicted for reference. For a fair comparison of the different prediction schemes, independent of the channel estimator used to deliver the predictors input, the performance when true channel samples are fed to the predictors $(\text{SNR} \to \infty)$ is shown. The performance degradation when the practical channel estimator of Section IV is used in conjunction with the R-BEM LRP proposed is also shown. It can be seen that the prediction horizon of the proposed predictor is better than the one corresponding to the AR predictor (MMSE)

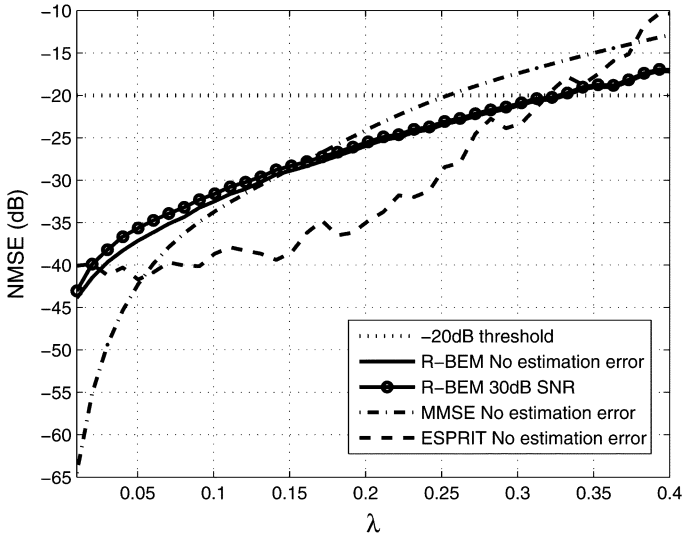

Fig. 6. NMSE performance for R-BEM LRP, MMSE LRP [13], and ESPRIT SOS predictor [44]. Predictors of [13] and [44] are fed with true channel samples $(\text{SNR} \to \infty)$ and R-BEM LRP with both true channel samples and 30 dB SNR estimated channel samples using (18). One frame prediction (22 symbols) is equivalent to $\lambda = 0.037$ and $\lambda = 0.222$ for mobile speeds of 10 km/h and 60 km/h respectively.

and similar to that of the SOS (ESPRIT). R-BEM LRP attains a prediction horizon of 0.33λ at the -20 dB threshold while the MMSE predictor and SOS predictor achieve 0.25 and 0.32λ respectively, being the performance of the R-BEM predictor better than that of the MMSE predictor from 0.15λ. The R-BEM predictor outperforms the MMSE predictor both in terms of low computational complexity and prediction range while having a prediction range comparable to the ESPRIT predictor at a much lower computational cost. For the given simulation parameters Table II shows the computational cost of the compared channel predictors. The number of complex operations for the predictor [43] was computed using a memory of 10 samples. For the ESPRIT predictor, the approximated computational cost provided in [35] was used for the evaluation of the coefficient update cost assuming that 6 nonzero channel taps are identified with an average of 8 rays each and a maximum of 16 rays per tap. We have that although the R-BEM-LRP results in only 30% computational saving for the given parameters, the complexity of the proposed predictor grows linearly with G while the complexity of [43], dominated by the coefficients update operation, grows quadratically with the predictor memory $\mathcal{M}$. Compared with the predictor in [35], the proposed scheme results in a computational saving of approximately 62%, without considering the initialization step required in [35].

Fig. 7 shows the performance of the proposed predictor when the channel Doppler spectrum does not follow the Jakes model. The Jakes Doppler result is plotted for comparison, together with a flat Doppler spectrum limited to ν_{dm}. Bandpass Doppler spectrum shapes were also tested. The wide bandpass Doppler spectrum is centered at ν_{dm} with a bandwidth of ν_{dm} and the narrow bandpass filter, also centered at ν_{dm} has a bandwidth of $0.3\nu_{dm}$. It can be seen that the results are very similar for all tested Doppler spectra which shows that the proposed technique is robust to non-Jakes Doppler spectrum as expected from the

TABLE II
COMPUTATIONAL COST EXAMPLE FOR THE SIMULATIONS SETTING

	Pred. Iteration	Coeff. Update
R-BEM proposed estim./pred.	$18,756$	-
RLS-MMSE pred. [43]	$3,824$	$22,953$
ESPRIT pred. [35]	$19,456$	$\approx 30,000$

A memory of 10 samples was used for the RLS-MMSE predictor. For the ESPRIT predictor, it is assumed that 6 nonzero channel taps are identified with an average of 8 rays each and a maximum of 16 rays per tap.

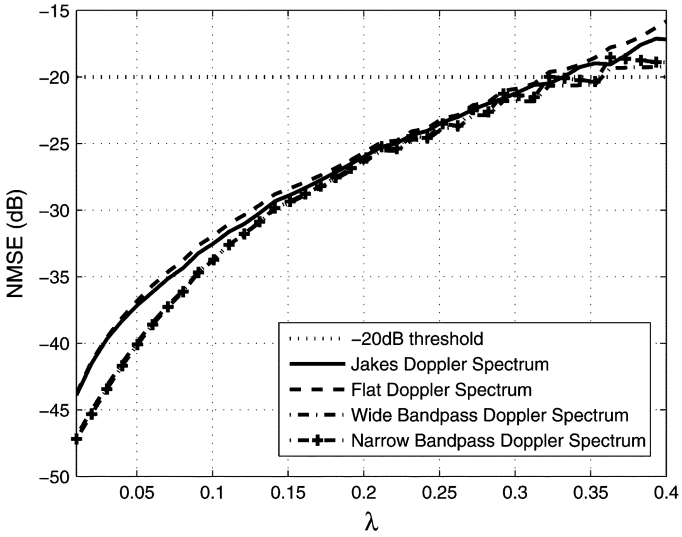

Fig. 7. NMSE versus λ performance for R-BEM LRP undergoing different Doppler shape channels. All curves attain the same prediction range showing that the prediction algorithm is robust to non-Jakes Doppler spectra. The predictor is fed with true channel samples (SNR $\rightarrow \infty$).

DCT approach. For this test the predictor is fed with true channel samples.

The above test with non-Jakes Doppler spectra was also carried out for the MMSE LRP and the ESPRIT predictor, and the results are shown in Fig. 8 along with the corresponding results of the R-BEM LRP. As expected, both the MMSE LRP and the ESPRIT predictor achieve roughly the same prediction horizons with the different Doppler spectra tested. These two predictors explicitly estimate the time domain autocorrelation function of the channel, and so they are robust to the Doppler model at the expense of increased computational load. On the other hand, the DCT modeling of the R-BEM LRP, makes the estimation of this autocorrelation function unnecessary thus avoiding the computational complexity involved.

Finally, Fig. 9 shows the performance of the R-BEM predictor as a function of SNR for a fixed prediction horizon of 1 frame (2 ms) for different mobile speeds. The curves show that the proposed predictor can reliably predict the channel one frame ahead from pedestrian to vehicular speeds for moderate to high SNR. The design objective of the proposed scheme prioritizes Doppler modeling before noise minimization. This enables to obtain low

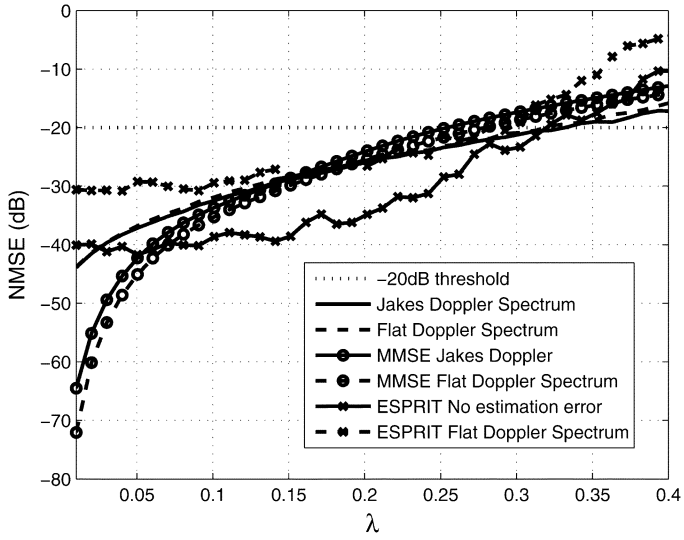

Fig. 8. NMSE versus λ performance for R-BEM LRP, MMSE LRP, and ESPRIT predictor undergoing different Doppler shape channels. Different from R-BEM LRP, the MMSE LRP and ESPRIT predictor explicitly estimate the time autocorrelation of the channel, leading to higher computational cost as compared to R-BEM LRP.

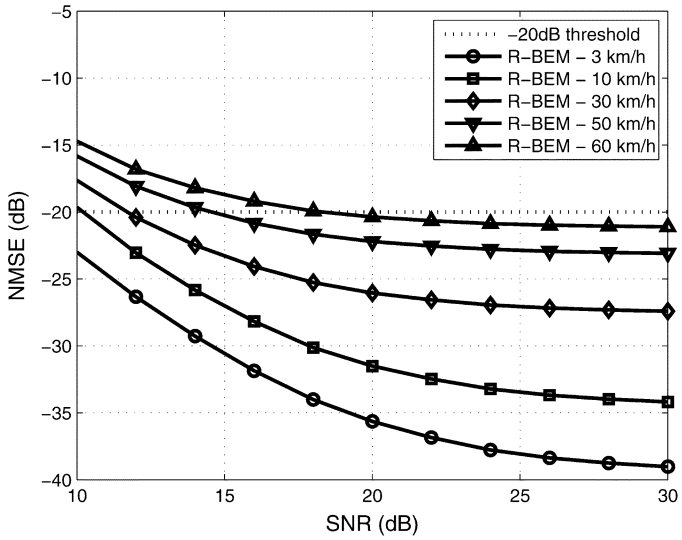

Fig. 9. NMSE versus SNR for R-BEM LRP at different mobile speeds and at a fixed prediction horizon of 1 frame. Mobile speeds of 3, 10, 30, 50, and 60 km/h correspond to fractions of λ equal to 0.011, 0.037, 0.111, 0.185, and 0.222 respectively.

complexity solutions to the prediction problem without sacrificing too much in modeling accuracy. Equation (5) gives an accurate value of G for a moderate to high SNR environment by discarding low energy basis coefficients more sensitive to noise. In a low SNR scenario more basis coefficients will be sensitive to noise and the classical more conservative criterion $G = \lceil 2\pi\nu_d M \rceil + 1$ results more appropriate for selecting the basis dimension G.

VIII. CONCLUSION

We proposed a recursive implementation for the basis expansion model (BEM) based on an approximation of the spectral characteristics of discrete cosine transform (DCT). This BEM formulation avoids the estimation and online updating of the

Doppler statistics of the time-varying channel. Moreover, it results in a time invariant structure that leads to a low complexity Kalman formulation of the estimation problem.

A long range channel predictor was derived from the proposed estimation structure. This predictor makes use of the good fitting properties of the estimators based on BEMs and the good prediction characteristic of recursive implementation. In addition, it renders low computational complexity as the proposed estimation structure is time invariant. Simulation results show that the proposed predictor is a good alternative for low complexity channel prediction at moderate to high SNR, because it attains a reliable prediction horizon comparable to that of the sum-of-sinusoids (SOS) prediction approach at a small fraction of the required computational cost of SOS.

REFERENCES

[1] 3GPP, Physical layer aspects for evolved UTRA 3GPP Tech. Rep. TR 25.814, Feb. 2006, Ver. 1.0.3.

[2] A. Molisch, L. Greenstein, and M. Shafi, "Propagation issues for cognitive radio," *Proc. IEEE*, vol. 97, no. 5, pp. 787–804, May 2009.

[3] M. Niedzwiecki, *Identification of Time-Varying Processes*. New York: Wiley, 2000.

[4] M. Tsatsanis and G. Giannakis, "Modeling and equalization of rapidly fading channels," *Int. J. Adaptive Control Signal Process.*, vol. 10, no. 2/3, pp. 159–176, Mar. 1996.

[5] T. Zemen and C. Mecklenbrauker, "Time-variant channel estimation using discrete prolate spheroidal sequences," *IEEE Trans. Signal Process.*, vol. 53, no. 9, pp. 3597–3607, Sep. 2005.

[6] Z. Tang, R. Cannizzaro, G. Leus, and P. Banelli, "Pilot-assisted time-varying channel estimation for OFDM systems," *IEEE Trans. Signal Process.*, vol. 55, no. 5, pp. 2226–2238, May 2007.

[7] P. Prakasam, M. Kulkarni, X. Chen, Z. Yu, S. Hoyos, J. Silva-Martinez, and E. Sanchez-Sinencio, "Applications of multipath transform-domain charge-sampling wide-band receivers," *IEEE Trans. Circuits Syst. II, Exp. Brief*, vol. 55, no. 4, pp. 309–313, Apr. 2008.

[8] K. Chen and T. Chiueh, "A cognitive radio system using discrete wavelet multitone modulation," *IEEE Trans. Circuits Syst I, Reg. Papers*, vol. 55, no. 10, pp. 3246–3258, Nov. 2008.

[9] L. Lindbom, "Simplified Kalman estimation of fading mobile radio channels: High performance at LMS computational load," in *Proc. IEEE ICASSP*, Apr. 1993, vol. 3, pp. 352–355.

[10] R. Bosisio, M. Nicoli, and U. Spagnolini, "Kalman filter of channel modes in time-varying wireless systems," in *Proc. IEEE ICASSP*, Mar. 2005, vol. 3, pp. iii/785–iii/788.

[11] W. Jakes, *Microwave Mobile Communications*. New York: Wiley, 1974.

[12] T. Zemen, C. Mecklenbrauker, and B. Fleury, "Time-variant channel prediction using time-concentrated and band-limited sequences," in *Proc. IEEE ICC*, Jun. 2006, vol. 12, pp. 5660–5665.

[13] T. Ekman, "Prediction of mobile radio channels," Ph.D. dissertation, Uppsala University, Uppsala, Sweden, 2002.

[14] T. Ekman, M. Sternad, and A. Ahlen, "Unbiased power prediction of Rayleigh fading channels," in *Proc. IEEE 56th VTC Fall*, 2002, vol. 1, pp. 280–284.

[15] M. Sternad and D. Aronsson, "Channel estimation and prediction for adaptive OFDM downlinks," in *Proc. IEEE 58th VTC Fall*, Oct. 2003, vol. 2, pp. 1283–1287.

[16] X. Zhao, J. Kivinen, P. Vainikainen, and K. Skog, "Characterization of Doppler spectra for mobile communications at 5.3 GHz," *IEEE Trans. Veh. Technol.*, vol. 52, no. 1, pp. 14–23, Jan. 2003.

[17] A. Duel-Hallen, "Fading channel prediction for mobile radio adaptive transmission systems," *Proc. IEEE*, vol. 95, no. 12, pp. 2299–2313, Dec. 2007.

[18] Y.-H. Yeh and S.-G. Chen, "Efficient channel estimation based on discrete cosine transform," in *Proc. IEEE ICASSP*, Apr. 2003, vol. 4, pp. IV-676–IV-679.

[19] Y.-H. Yeh and S.-G. Chen, "DCT-based channel estimation for OFDM systems," in *Proc. IEEE ICC*, Jun. 2004, vol. 4, pp. 2442–2446.

[20] H. Kobayashi and K. Mori, "Proposal of OFDM channel estimation method using discrete cosine tramsform," in *Proc. IEEE 15th PIMRC*, Sep. 2004, vol. 3, pp. 1797–1801.

[21] P. Tan and N. Beaulieu, "A comparison of DCT-based OFDM and DFT-based OFDM in frequency offset and fading channels," *IEEE Trans. Commun.*, vol. 54, no. 11, pp. 2113–2125, Nov. 2006.

[22] S. Kim, H. Yu, J. Lee, and D. Hong, "Low bias frequency domain SNR estimator using DCT in mobile fading channels," *IEEE Trans. Wireless Commun.*, vol. 8, no. 1, pp. 45–50, Jan. 2009.

[23] N. Al-Dhahir, H. Minn, and S. Satish, "Optimum DCT-based multicarrier transceivers for frequency-selective channels," *IEEE Trans. Commun.*, vol. 54, no. 5, pp. 911–921, May 2006.

[24] B. Jiang, W. Wang, H. Wang, and X. Gao, "Two dimensional DCT-based channel estimation for OFDM systems with virtual subcarriers in mobile wireless channels," in *Proc. IEEE ICC*, May 2008, pp. 3801–3806.

[25] M. Zhou, B. Jiang, T. Li, W. Zhong, and X. Gao, "DCT-based channel estimation techniques for LTE uplink," in *Proc. IEEE PIMRC*, 2009, pp. 1034–1038.

[26] M. Diallo, R. Rabineau, L. Cariou, and M. Helard, "On improved DCT based channel estimation with very low complexity for MIMO-OFDM systems," in *Proc. IEEE VTC*, 2009, pp. 1–5.

[27] Z. Zhang, S. Chan, and K. Tsui, "A recursive frequency estimator using linear prediction and Kalman-filter-based iterative algorithm," *IEEE Trans. Circuits Syst. II, Exp. Briefs*, vol. 55, no. 6, pp. 576–580, Jun. 2008.

[28] B. Liao, Z. Zhang, and S. Chan, "A robust Kalman filter-based subspace tracking algorithm in an impulsive noise environment," *IEEE Trans. Circuits Syst. II, Exp. Briefs*, vol. 57, no. 9, pp. 740–744, Sep. 2010.

[29] K. Muralidhar and K. H. Li, "A low-complexity Kalman approach for channel estimation in doubly-selective OFDM systems," *IEEE Signal Process. Lett.*, vol. 16, no. 7, pp. 632–635, Jul. 2009.

[30] M. Sternad, T. Ekman, and A. Ahlen, "Power prediction on broadband channels," in *Prof. IEEE 53rd VTC Spring*, 2001, vol. 4, pp. 2328–2332.

[31] R. Negi and J. Cioffi, "Pilot tone selection for channel estimation in a mobile OFDM system," *IEEE Trans. Consum. Electron.*, vol. 44, no. 3, pp. 1122–1128, Aug. 1998.

[32] X. Cai and G. Giannakis, "Bounding performance and suppressing intercarrier interference in wireless mobile OFDM," *IEEE Trans. Commun.*, vol. 51, no. 12, pp. 2047–2056, Dec. 2003.

[33] L. Rugini, P. Banelli, and G. Leus, "Low-complexity banded equalizers for OFDM systems in Doppler spread channels," *EURASIP J. Appl. Signal Process.*, vol. 2006, p. 13, Apr. 2006.

[34] P. A. Regalia, *Adaptive IIR Filtering in Signal Processing and Control*. New York: Marcel Dekker, 1995.

[35] I. Wong and B. Evans, "Low-complexity adaptive high-resolution channel prediction for OFDM systems," in *Proc. IEEE GLOBECOM*, Dec. 1, 2006, vol. 27, pp. 1–5.

[36] H. Chiang and J. Liu, "A novel DCT-based prefilter structure for efficient digital filter design," *Signal Process.*, no. 54, pp. 249–260, May 1996.

[37] P. Regalia, "An improved lattice-based adaptive IIR notch filter," *IEEE Trans. Signal Process.*, vol. 39, no. 9, pp. 2124–2128, Sep. 1991.

[38] C. Chui and G. Chen, *Kalman Filtering—With Real-Time Applications*, 2nd ed. New York: Springer-Verlag, 1991.

[39] I. Arnold, W. F. , and A. Laub, "Generalized eigenproblem algorithms and software for algebraic Riccati equations," *Proc. IEEE*, vol. 72, no. 12, pp. 1746–1754, 1984.

[40] A. Duel-Hallen, S. Hu, and H. Hallen, "Long-range prediction of fading signals," *IEEE Signal Process. Mag.*, vol. 17, no. 3, pp. 62–75, May 2000.

[41] J. Schmidt, J. Cousseau, R. Wichman, and F. Gregorio, "Fast-fading channel estimator using DCT and simplified Kalman filter," in *Proc. IEEE 8th SPAWC*, Jun. 2007, pp. 1–5.

[42] D. Tse and P. Viswanath, *Fundamentals of Wireless Communication*. Cambridge, U.K.: Cambridge Univ. Press, 2004.

[43] D. Schafhuber and G. Matz, "MMSE and adaptive prediction of time-varying channels for OFDM systems," *IEEE Trans. Wireless Commun.*, vol. 4, no. 2, pp. 593–602, Mar. 2005.

[44] I. Wong and B. Evans, "Joint channel estimation and prediction for OFDM systems," in *Proc. IEEE GLOBECOM*, Dec. 2005, vol. 4, pp. 2255–2259.

[45] S. Semmelrodt and R. Kattenbach, "Investigation of different fading forecast schemes for flat fading radio channels," in *Proc. IEEE 58th VTV Fall*, Oct. 2003, vol. 1, pp. 149–153.

Jorge F. Schmidt (S'06–M'10) received the B.Sc. degree in electrical engineering from the Universidad Nacional del Sur (UNS), Bahía Blanca, Argentina, in 2005. He is currently working toward the Ph.D. degree with the Signal Processing and Communication Laboratory (LaPSyC), UNS.

His research interests are in the areas of adaptive filtering and statistical signal processing for multiuser communication systems.

Juan E. Cousseau (S'90–M'92–SM'00) received the B.Sc. degree in electrical engineering from the Universidad Nacional del Sur (UNS), Bahia Blanca, Argentina, in 1983 and the M.Sc. and Ph.D. degrees in electrical engineering from COPPE/ Universidade Federal do Rio de Janeiro (UFRJ), Brazil, in 1989 and 1993, respectively.

Since 1984, he has been with the undergraduate department of Electrical and Computer Engineering at UNS. He has also been with the graduate program at the same university since 1994. He is Coordinator of the Signal Processing and Communication Laboratory (LaPSyC) at UNS. He is a Senior Researcher with the National Scientific and Technical Research Council (CONICET) of Argentina. He has been involved in scientific and industry projects with research groups from Argentina, Brazil, Spain, and the United States. He was a Visiting Professor at the University of California, Irvine, in 1999 and the Signal Processing Laboratory, Helsinki University of Technology, in 2004 and 2006.

Dr. Cousseau was IEEE Circuits and Systems Chair of the Argentine Chapter from 1997 to 2000, and member of the Executive Committee of the IEEE Circuits and Systems Society during 2000/2001 (vice president for Region 9). He participated in the IEEE Signal Processing Society Distinguished Lecturer Program in 2007.

Risto Wichman received the M.Sc. and D.Sc. (Tech.) degrees in digital signal processing from Tampere University of Technology, Tampere, Finland, in 1990 and 1995, respectively.

From 1995 to 2001, he worked at Nokia Research Center as a Senior Research Engineer. In 2002, he joined Department of Signal Processing and Acoustics, Faculty of Electrical Engineering, Aalto University, Aalto, Finland, where he has been a Professor since 2003. His research interests include digital signal processing for wireless communications systems.

Stefan Werner (S'98–M'03–SM'07) received the M.Sc. degree in electrical engineering from the Royal Institute of Technology (KTH), Stockholm, Sweden, in 1998 and the D.Sc. (EE) degree (with honors) from the Signal Processing Laboratory, Smart and Novel Radios (SMARAD) Center of Excellence, Helsinki University of Technology (TKK), Espoo, Finland, in 2002.

He is currently an Academy Research Fellow in the Department of Signal Processing and Acoustics, Aalto University, Finland, where he is also appointed as a Docent. His research interests include adaptive signal processing, signal processing for communications, and statistical signal processing.

Dr. Werner is a member of the editorial board of *Signal Processing*.